Aalborg Universitet

AALBORG UNIVERSITY

Performance Analysis of Single-Phase Electrical Machine for Military Applications

Ganesan, Aswin Uvaraj; Nandhagopal, Sathyanarayanan; Venkat, Arvind Shiyam; Padmanaban, Sanjeevikumar; Pedersen, John K.; Chokkalingam, Lenin Natesan; Leonowicz, Zbigniew

Performance Analysis of Single-Phase Electrical Machine for Military Applications

Aswin Uvaraj Ganesan [1], Sathyanarayanan Nandhagopal [1], Arvind Shiyam Venkat [1], Sanjeevikumar Padmanaban [2] , John K. Pedersen [3], Lenin Natesan Chokkalingam [1,*] and Zbigniew Leonowicz [4]

[1] School of Electrical Engineering, Vellore Institute of Technology (VIT) University, Chennai, Tamilnadu 600127, India; aswin.uvaraj2013@vit.ac.in (A.U.G.); sathyanarayanan.n2014@vit.ac.in (S.N.); venk5arvind@gmail.com (A.S.V.)

[2] Department of Energy Technology, Aalborg University, Esbjerg 6700, Denmark; san@et.aau.dk

[3] Department of Energy Technology, Aalborg University, Aalborg 9220, Denmark; jkp@et.aau.dk

[4] Department of Electrical Engineering, Wroclaw University of Technology, Wyb. Wyspianskiego 27, I-7, 50370 Wroclaw, Poland; zbigniew.leonowicz@pwr.edu.pl

[*] Correspondence: lenin.nc@vit.ac.in; Tel.: +91-944-450-6077

Abstract: A permanent magnet assisted synchronous reluctance generator (PMA-SynRG) and an induction generator (IG) were compared for portable generator applications. PMA-SynRG with two rotor configurations, namely rotors with ferrite magnet and NdFeB, were designed. Furthermore, a design strategy for both PMA-SynRG and IG is presented with their geometrical dimensions. The machine was designed and results were analyzed using finite element analysis. Results such as flux density, open circuit and full load voltages, torque in generating mode, weight comparison and detailed cost analysis were investigated. In addition, thermal analysis for various ambient conditions (−40 °C, +30 °C, +65 °C) was evaluated for both PMA-SynRG and IG. Furthermore, acoustic versus frequency plot and acoustic pressure level were investigated for both the generators. Finally, the results confirmed that the machine with a higher power-to-weight ratio was the right choice for military applications.

Keywords: permanent magnet assisted synchronous reluctance generator; induction generator; ferrite; military applications; portable generator

---

1. Introduction

A portable generator, or compact generator, is a gasoline-driven engine, alternating current (AC) generator. The power range of these types of generators lies between 1–11 kW, depending on industry standards [1]. It is designed to supply electrical power for lighting, appliances, tools and low or medium power equipments [2]. The dissembled view of a portable generator is presented in Figure 1. In recent periods, the need for compact generators is largely expanded [3]. This kind of generator can be more useful during power failures through unavoidable circumstances [4]. Portable generators use small engines in which the spinning shaft of the engine creates an alternating magnetic field through a coil which induces voltage [5]. Light weight and high power are the key factors of portable generators.

The permanent magnet synchronous generators (PMSG) are an appropriate choice for portable generators in military usage, due to their high power density, compact size and high efficiency. Permanent magnet (PM) is a replacement of field winding in conventional machines [6].

Rare earth magnets are commonly divided into light rare earth magnets and less-available heavy rare earth magnets [7]. The most plenteous rare earth magnets are lanthanum, cerium, and neodymium, which are all considered light earth magnets, along with praseodymium and samarium [8].

The most common PMs are samarium cobalt and neodymium-iron-boron. Samarium cobalt magnets perform well at higher temperatures but are brittle, which confines magnet size and can cause issues with certain motoring applications [9].

Neodymium–iron–boron magnets are significantly stronger than samarium cobalt magnets. As a result, their size is not as limited and they are more appropriate for generator applications. These magnets normally have two to four percent of dysprosium to enhance their temperature resistance [4]. Nearly 90% of high-value rare earth magnets are from China [10], which makes the design using PMs very costly [11].
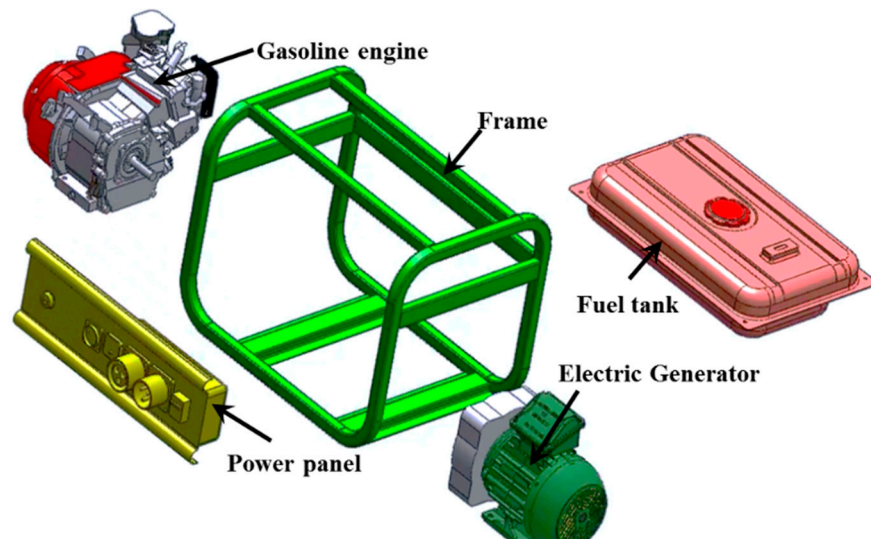
Figure 1. Dissembled view of portable generator.

The Permanent Magnet Synchronous Reluctance Generator (PMA-SynRG) is similar to a synchronous reluctance generator and costs less than the PMSG [12], which is also used in various applications [13]. In a PMA-SynRG, PMs are placed in the flux barriers, creating a magnet torque which supports and increases the torque characteristics [14]. Moreover, the usage of PMs will increase the power factor in combination with SynRG. The volume, type, and positioning of PMs differ widely from PMA-SynRG [15]. The magnet material used is of rare earth magnets and ferrite magnets. Ferrite magnets, also known as ceramic magnets, are alloys of Barium (Ba) or Strontium (Sr) with ferrite (Fe_2O_3). The materials have a linear demagnetization characteristic and cost less which makes them the most common magnets for general purpose applications [16] (refer to Appendix A Table A1).

Similarly, the induction generator (IG) is also a better choice for portable generators [17] where weight is a major concern. Ruggedness, simple design, robustness, lower cost, and reduced maintenance are the most important benefits of IG. The presence of residual flux in the rotor core and the excitation capacitance self-excites IG, causing the stator voltage to build up [18].

This research work concentrates mainly on the performance and weight comparison of PMA-SynRG and IG to meet the military standards. Three generator topologies (ferrite rotor, NdFeB rotor and IG) were designed and investigated. The rotor with an NdFeB magnet performed better and has a 21.57% higher power–to–weight ratio in comparison to IG. Furthermore, a detailed cost analysis was provided disclosing that IG reduced costs in comparison to the topology of other generators. The noise levels of both the NdFeB rotor and IG are of military standards. Finally, these two generator configurations confirmed a 20%–30% rate of reduced weight compared with an existing 5 kW generator in the military applications.

Section 2 explains the constraints and requirements of a portable generator in military applications. Section 3 deals with the design strategy of PMA-SynRG and IG. In Section 4, the stator and rotor geometrical configurations, output voltage waveform, torque in generating mode, weight comparison

cost analysis, and overall performance characteristics are evaluated using finite element analysis (FEA). Section 5 covers the thermal analysis for various ambient temperatures and also highlights the acoustic pressure level of both generators. Section 6 deals with a detailed cost estimation of the machine. Finally, Section 7 concludes with the kW/kg difference of NdFeB rotor and other configurations.

2. Constraints of Portable Generator in Military Applications

Size, weight, and price are the key factors in designing an electric machine for military applications. Prominent performance developments in IG and price deductions of PM materials in PMA-SynRG make them more appropriate for military usage. IG and PMA-SynRG provide following features, such as reduced weight and size, simple mechanical structure, less maintenance, good reliability, and better efficiency. The requirements are tabulated as per standard –MIL–STD–1332B (see Table 1).

Table 1. As per military standards.

Characteristic	Value 5 kW
Weight, (dry)	750 lbs. (340.2 Kg)
Weight, wet, 80% fueled	796 lbs. (361.1 Kg)
Noise	68 dBA
Dimensions	$45 \times 32 \times 36$ in ($1.143 \times 0.813 \times 0.914$ m)
Thermal ambient conditions	$-42\,°C$ to $+65\,°C$

3. Design Strategy for Portable Generator

### 3.1. Permanent Magnet Synchronous Reluctance Generator

The design procedure of PMA-SynRG consists of following steps:

I.   The barrier number, size, position and shape are optimized for required output voltage and good saliency ratio.

II.   The magnets are designed and placed to meet the PM flux linkage required for this application.

The count of flux barrier is optimized as five per pole. Increasing the barrier count greater than five does not have key variations in the saliency ratio related to stator slots and barrier geometries [19,20]. Further increasing the number of flux barrier greater than five imposes mechanical problems with respect to rotor geometry [21].

The rotor topology and the polarization of the magnets are presented in Figure 2. The rotor design (the PM dimensions) was modelled with the help of numerical analysis with five flux barrier per pole to increase saliency and reduce cogging torque.
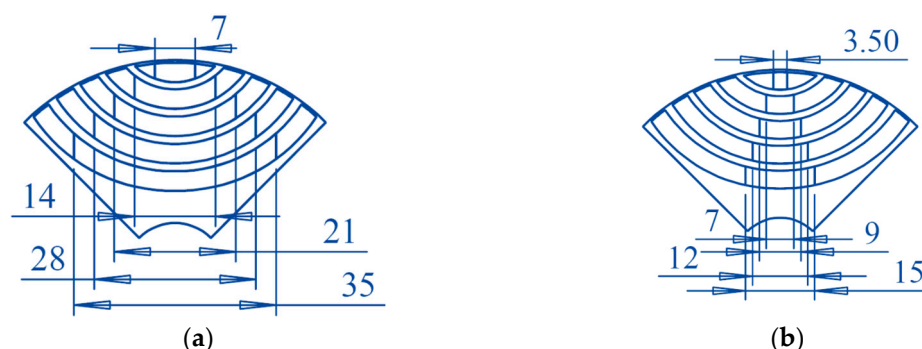
Figure 2. Geometrical dimensions of PMA-SynRG, (**a**) ferrite (G1), (**b**) NdFeB (G2).

3.2. Induction Generator

The presence of residual flux in the rotor core and the excitation capacitance self-excites IG, causing the stator voltage to build up. The excitation capacitance is calculated as follows:

Apparent power

$$P_A = \frac{P}{\cos \theta} \tag{1}$$

Reactive power

$$P_R = \sqrt{P_A{}^2 - P^2} \tag{2}$$

From the reactive power, the necessary capacitive current (I_{cap}), reactance (X_{cap}) and capacitance (C) of the capacitor are calculated from the given equations:

$$I_{Cap} = \frac{P_R}{V_{term}} \tag{3}$$

$$X_{Cap} = \frac{V_{term}}{I_{cap}} \tag{4}$$

$$C = \frac{1}{2 \pi f X_{cap}} \tag{5}$$

From the machine parameters, Equations (1)–(5), the capacitor value is fixed as 400 μF, 400 V. The rotor of IG, designed with the help of finite elements, is displayed in Figure 3.

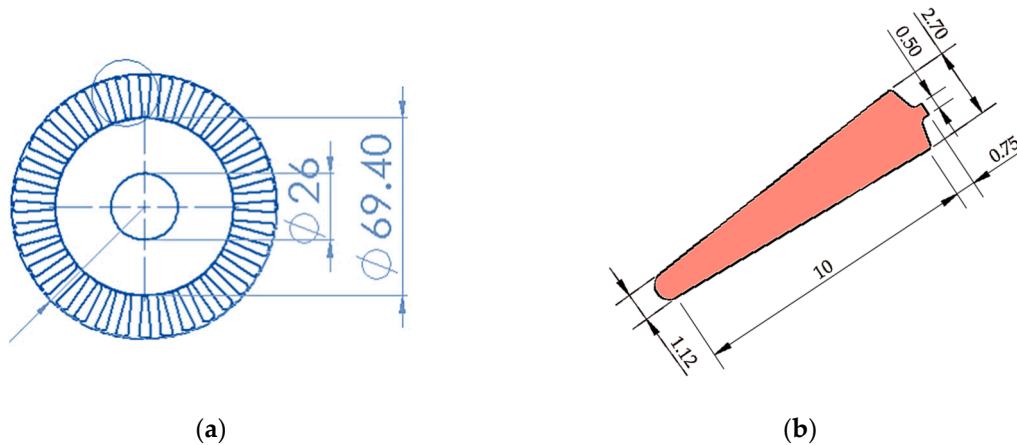**(a)**   **(b)**

Figure 3. Geometrical dimensions of induction generator. (**a**) Rotor core, (**b**) Rotor bar.

4. Finite Element Analysis

A single phase PMA-SynRG and IG were designed for portable applications with a 48 slot stator. The rotor with ferrite (G1), NdFeB magnet (G2) and IG (G3) is presented in Figure 4. The stator with distributed windings was used for all three machine configurations, i.e., the same dimensions (except stack length). The design requirement of the machine is tabulated in Table 2. The output characteristics of the modelled generator connected to a resistive load were simulated by MagNet software. During the pre-processing stage, the analytical design was modelled. Subsequently, the material was assigned and the triangular mesh region created. The mesh was denser in the air gap region so as to accurately analyze the effects of air gap flux density (Refer to Figure 5). The meshed design of G1 was 29,304 nodes and 58,306 elements, whereas for G2 it was 27,204 nodes and 54,370 elements. Furthermore, the G3 has 33,086 nodes and 66,134 elements. Transient with motion analysis was performed with designed source circuit.

Table 2. Design requirements.

Parameters	Unit	Value		
Output power	kW	5		
Speed	rpm	1500		
Voltage	V	230		
Frequency	Hz	50		
No. of phase	-	1ϕ		
No of poles	-	4		
Outer stator diameter	mm	125		
Inner stator diameter	-	85		
Magnet thickness	mm	5		
Load resistance	Ω	10.6		
Stack length	mm	G1 118	G2 75	G3 91

(a)

(b)

(c)

(d)
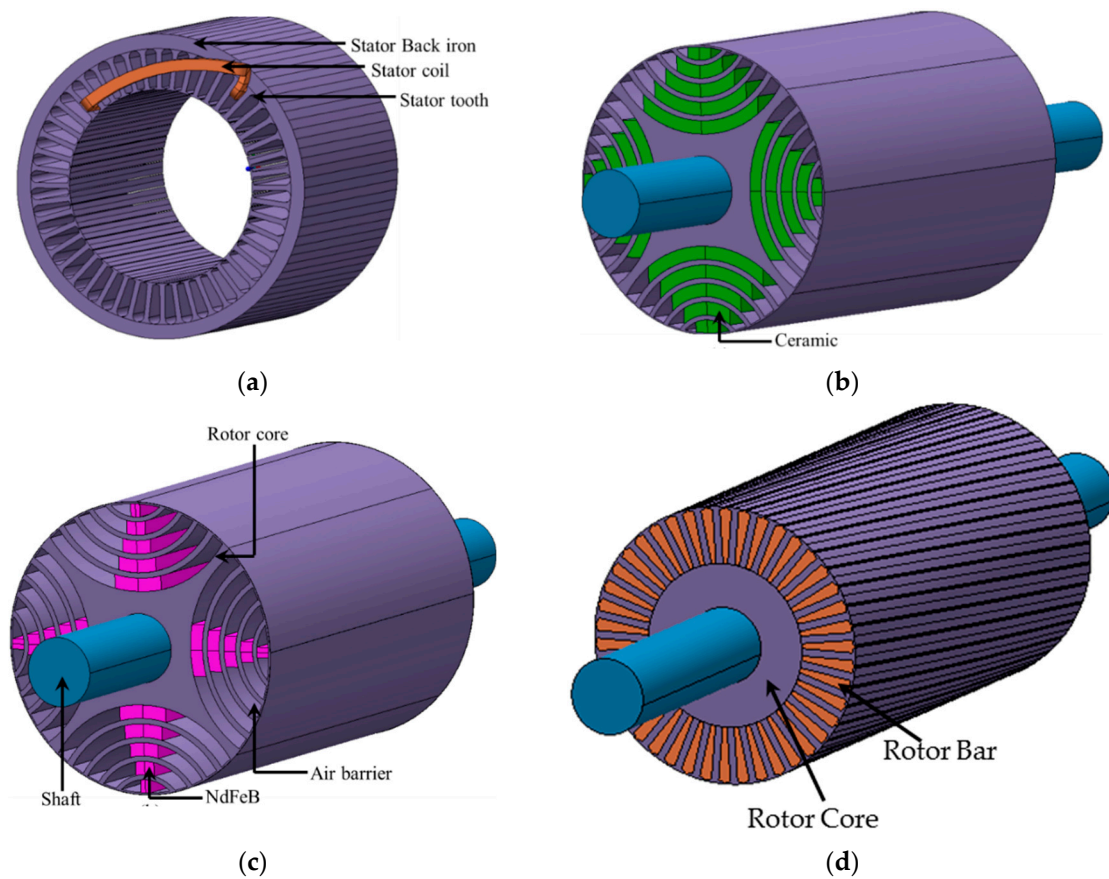
Figure 4. SynRG with: (**a**) stator, (**b**) ferrite rotor, (G1), (**c**) NdFeB rotor (G2), (**d**) IG (G3).
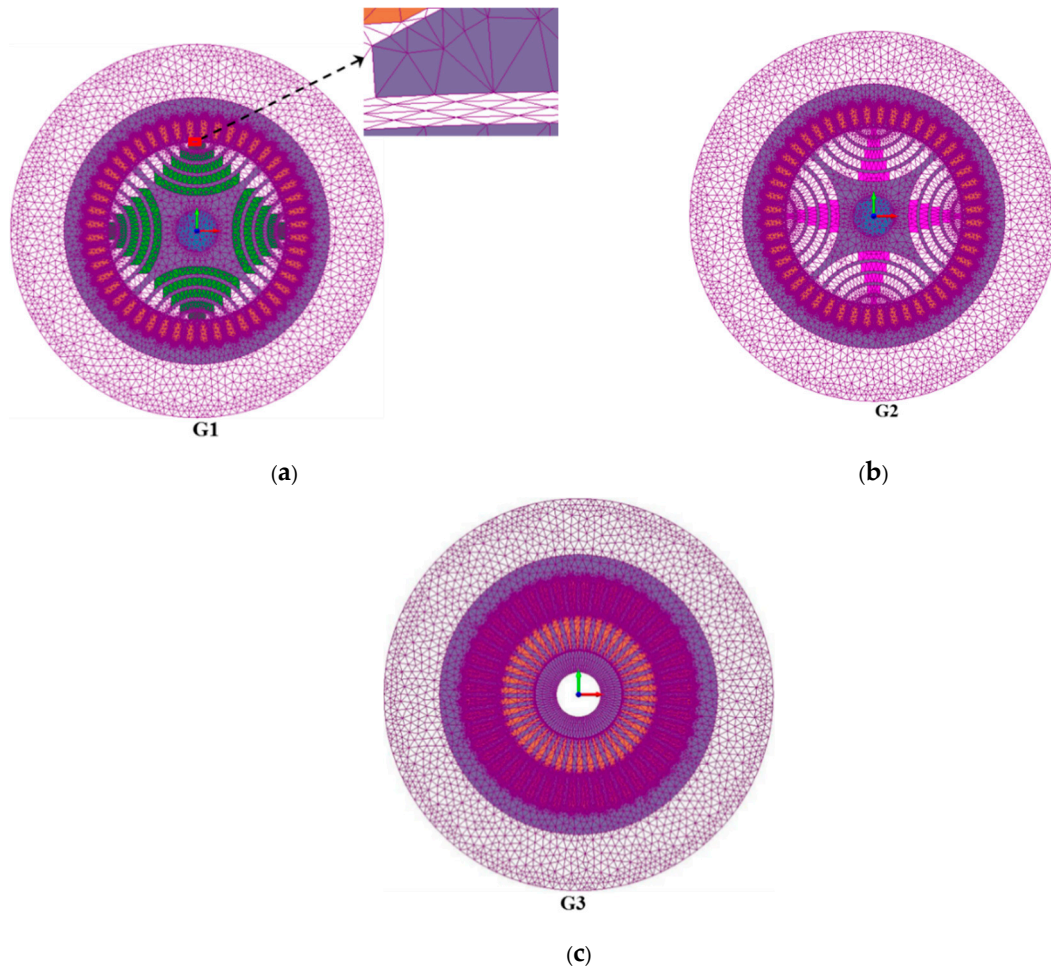
Figure 5. Mesh generation of G1, G2, and G3.

4.1. Flux Distribution

In PMA-SynRG, the direct and quadrature axes flux linkages can be represented as
d-axis flux linkage:

$$\lambda_d \ = \ L_d i_d \tag{6}$$

q-axis flux linkage:

$$\lambda_q \ = \ L_q i_q - \Lambda_{pm} \tag{7}$$

where Λ_{pm} represents the PM flux linkage, L_d and L_q are *d*- and *q*-axes inductances, respectively. Similarly i_d and i_q are corresponding *d*- and *q*-axes currents.

In Figure 6, the magnetic flux density for G1, G2, and G3 are presented, where G3 has a maximum flux density of 1.36 Wb/m^2.
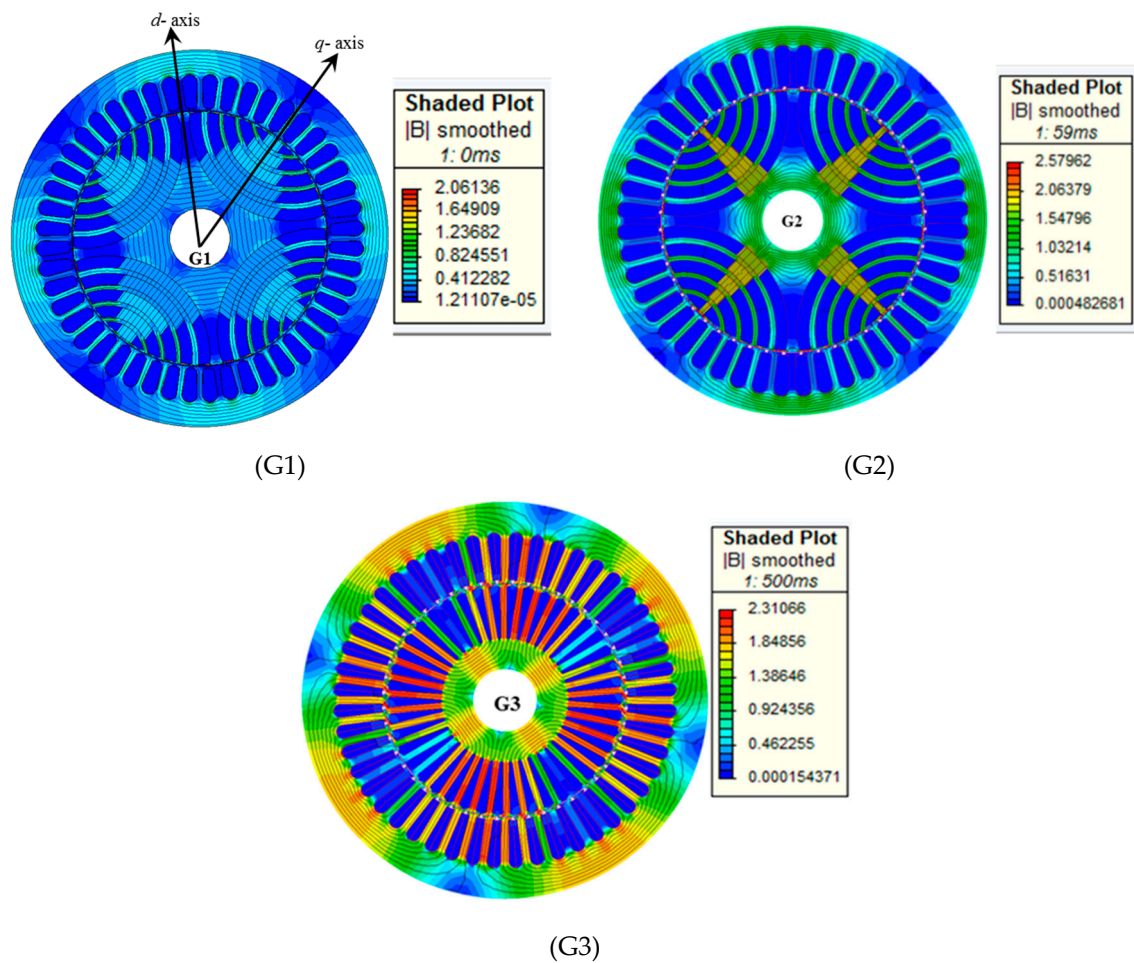
(G1)　　　　　　　　　　　　　　　　　　　　(G2)

(G3)

Figure 6. Flux density plot for G1, G2, and G3.

4.2. Output Voltage Waveforms

The aim of a generator design is to generate stator voltage which almost looks like a sinusoidal waveform with a minimal harmonic content, which minimizes the losses in the generator. In Figure 7, stator-winding peak–peak voltage under resistive load condition for G1, G2, and G3 is presented. During no-load operation, the peak–peak voltage of 359 V is generated in G2, whereas it is 384 V in G3, respectively.
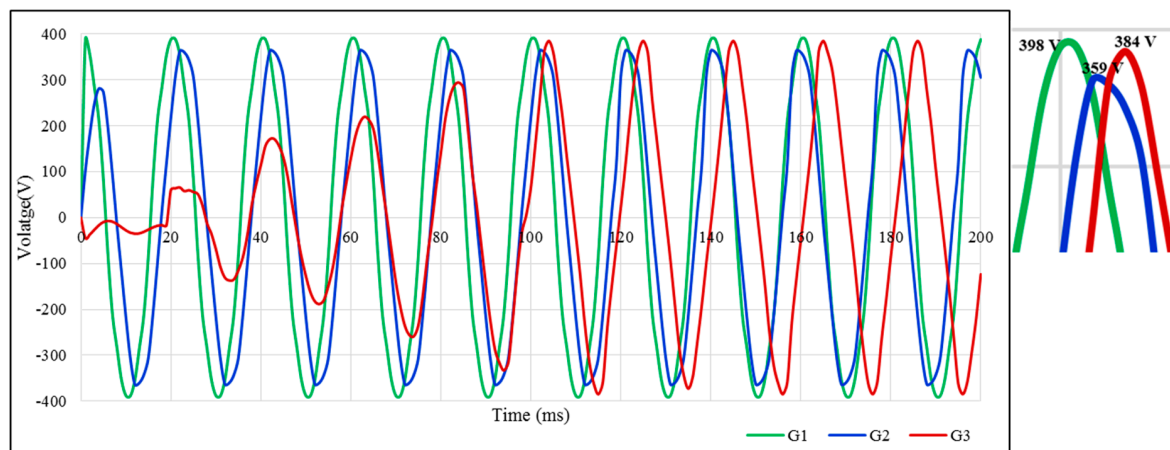

Figure 7. No-load voltage of G1, G2, and G3.

At full load condition, the voltage generated in G2 was 326 V peak–peak voltages, as shown in Figure 8, while in G1 it was 324 V. Moreover, transients voltages from the stator windings at full load condition were obtained with the excitation capacitor in G3, where the excitation capacitor was Ce = 400 μF. The voltage values confirm that the voltage regulation of G2 was better when compared with G1 and G3. Furthermore, the waveforms show that while using ferrite magnet the harmonics were higher compared to G2 topology.
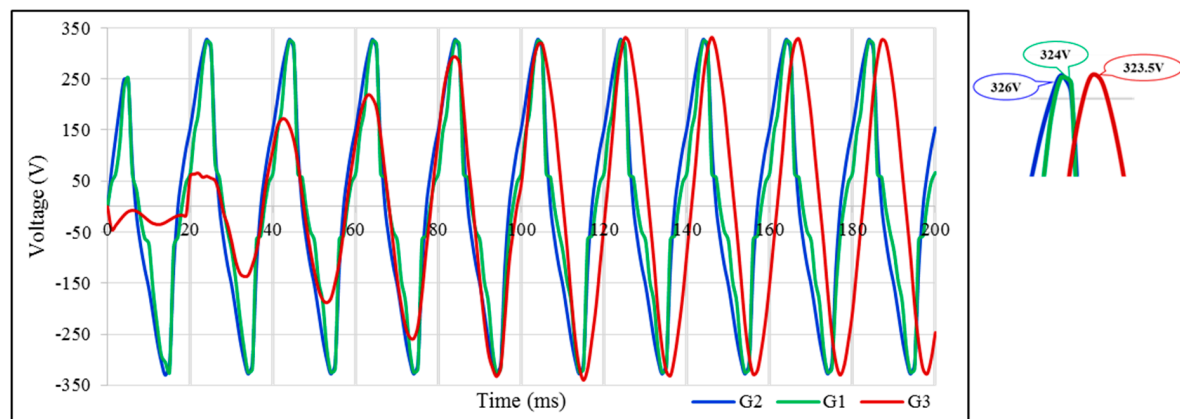

Figure 8. Full load voltage of G1, G2, and G3.

4.3. Weight of the Generators

As stated above, G2 has exactly the same structure as G1 and G3 except for the stack length which is 30.5% and 15.2% higher than G2. Accordingly, the weight of the active material and core material are not similar. The amount of PM used in G1 to achieve the required output was 72.2% higher than the G2 configuration. The reason behind this is NdFeB, which produces energy that is eleven times higher than that of the ferrite (about 367 kJ/m3 versus 32.9 kJ/m3) [22], resulting in the stack length of the machine to increase in order to achieve the required power, increasing the overall weight of G1. The overall weight comparison of each component of G1, G2, and G3 are displayed in Figure 9. These results confirm that the ferrite rotor (G1) was not a feasible machine for military applications, where weight plays a major role. The overall weight of G1 was 39.44% and 52% higher than G3 and G2, respectively. The further mechanical comparison was analyzed for G2 and G3 rotor configurations.
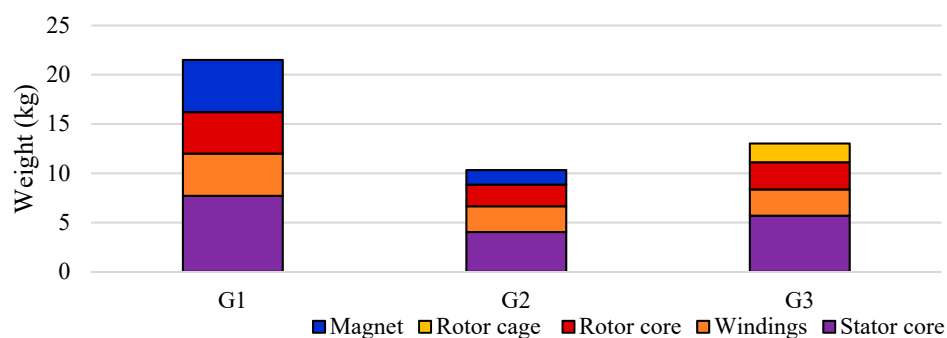

Figure 9. Weight comparison of G1, G2, and G3.

5. Mechanical Analysis

5.1. Transient Thermal Analysis

In a hollow cylinder containing a heat source, conductive heat transfer with various boundary conditions was obtained from the Fourier law in the cylindrical coordinate as [23]

$$\frac{1}{r}\frac{\partial}{\partial r}\left(kr\frac{\partial T}{\partial r}\right) + \frac{1}{r^2}\frac{\partial}{\partial \theta}\left(k\frac{\partial T}{\partial \theta}\right) + \frac{\partial}{\partial Z}\left(k\frac{\partial T}{\partial Z}\right) + q = \rho c \frac{dT}{dt} \tag{8}$$

Thermal analysis was carried out for 5 kW PM-SynRG with NdFeB (G2) and IG (G3). This FEA analysis dealt primarily with heat conduction through the generator components. The quantity of heat transmitted from the excited phase to surrounding regions primarily depended upon convection heat transfer coefficients, *h*. The value of '*h*' depends on thermal conductivity, specific heat, fluid dynamic viscosity and other properties of the coolant. The set of dimensionless numbers used in the calculation of convection heat transfer coefficients are given in Table 3.

In the Appendix A, Table A2 depicts the thermal properties for different materials used in G2 and G3 for thermal analysis. For the mesh region in Figure 10, G2 has 63,039 nodes and 121,776 elements, whereas for G3 has 69,739 nodes and 134,720 elements.

Table 3. Dimensionless parameters to calculate heat transfer coefficient [24].

Dimensionless Number	Equation	Nomenclature
Reynold's number	$Re = \frac{\prod D^2 \omega}{v}$	*D*—Diameter of the stator up to the stator pole arc (m) *ω*—Angular velocity = 2 $\prod$ N/60 (rad/s) *N*—Speed of the motor (rpm) *v*—Kinematic viscosity (m²/s)
Grashof number	$Gr = \frac{\beta g \theta \rho^2 L^3}{\mu^2}$	*β*—Coefficient of cubical expansion of fluid (K⁻¹) *g*—Gravitational force of attraction (m/s²) *θ*—Temperature difference between surface and fluid (K) *ρ*—Fluid density (kg/m³)
Prandtl number	$Pr = \frac{c\mu}{\lambda}$	*L*—Characteristic length of the surface (m) *μ*—Fluid dynamic viscosity (Kg/m s) *c*—Specific heat capacity of fluid (J/Kg K)
Nusselt Number	$h = \frac{Nu(\lambda)}{L}$	*λ*—Thermal conductivity of fluid (W/m K)
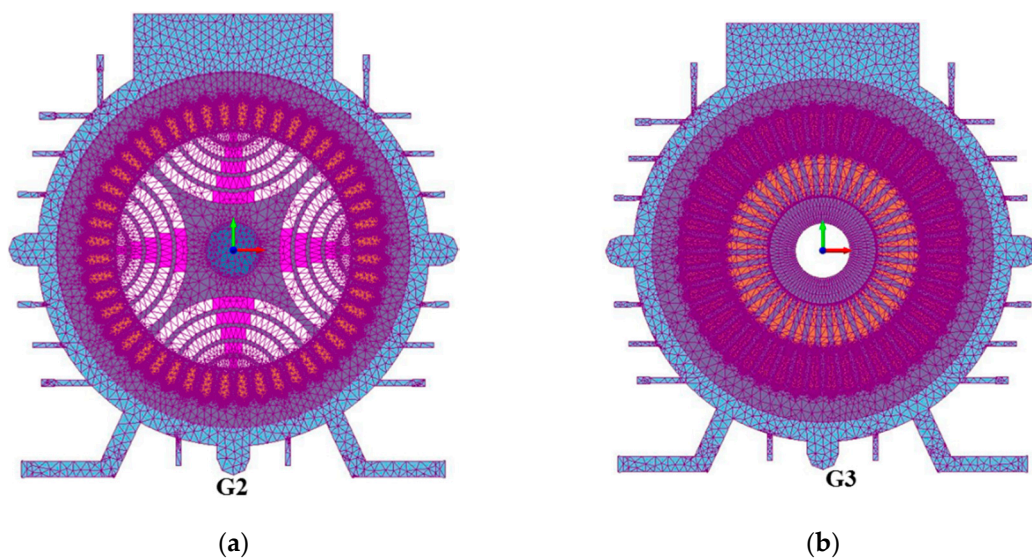
Figure 10. Mesh region with outer frame for (**a**) G2 and (**b**) G3.

From the electromagnetic analysis, the core loss and copper loss of G2 and G3 are calculated and tabulated for full load condition in Table 4. These losses are incorporated as input in thermal analysis to estimate the maximum temperature rise in G2 and G3.

Table 4. Electromagnetic losses.

Components	Heat Loss	
	G2	**G3**
Copper loss	491	833
Core loss	35	33

The thermal analysis was performed for ambient temperatures of +30 °C. The transient thermal analysis was performed for a duration of 6 h. The estimated temperature distribution in the generator for full load (100% load) condition is presented in Figure 11.

For full load in G2, it was noted that the temperature ranged from 94 °C to 100 °C, with the maximum temperature occurring on the stator winding. For full load in G3, it was noted that the temperature ranged from 118 °C to 132 °C, with the maximum temperature occurring on the rotor bar.


(**a**)   (**b**)
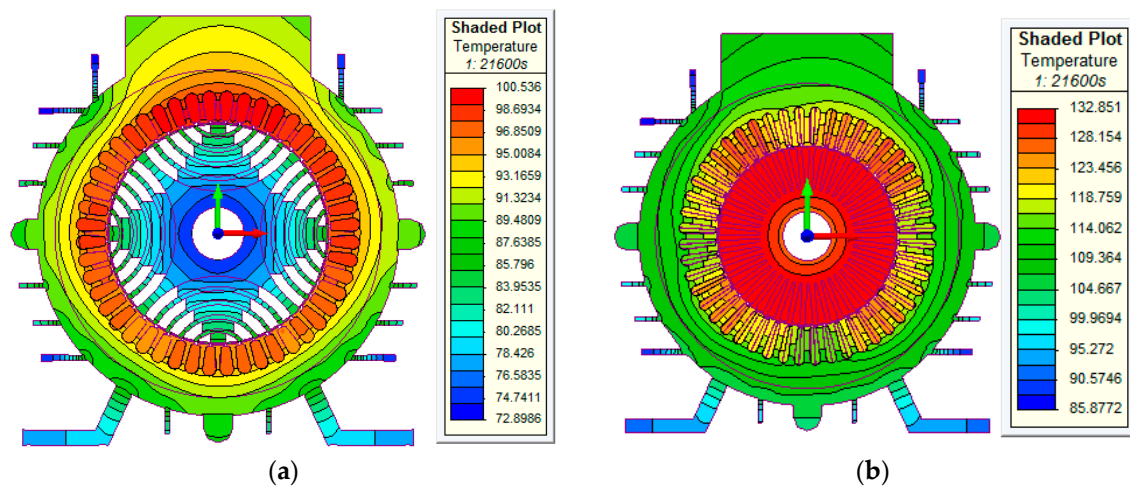
Figure 11. Temperature distribution for (**a**) G2 and (**b**) G3 (+30 °C ambient temperature). * All units are in °C.

The temperature distribution of G2 and G3 for the various ambient conditions (−40 °C, +30 °C +65 °C), is shown in Figures 12 and 13. At −40 °C, temperature in housing frame is −5.12 °C and −8.56 °C for G3 and G2, respectively.
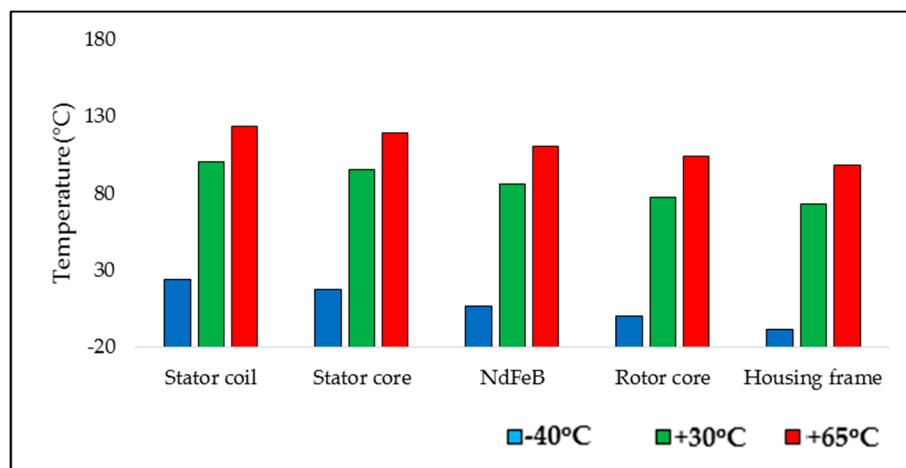
Figure 12. Temperature distribution of G2 for various ambient conditions (−40 °C, +30 °C, +65 °C).
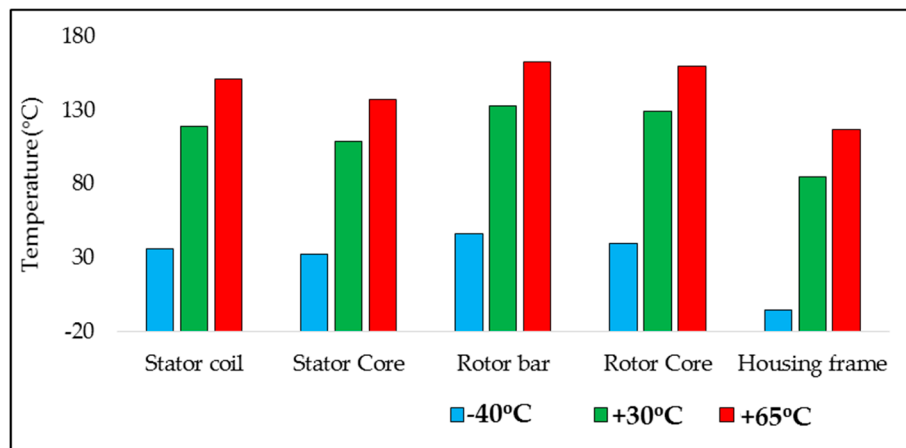
Figure 13. Temperature distribution of G3 for various ambient conditions (−40 °C, +30 °C, +65 °C).

5.2. Torque Waveform in Generating Mode

Figure 14 displays the FEA evaluated electromagnetic torque during generating operation. Furthermore, it was observed that the peak to peak torque ripple of G2 was 9% less than G3. The barrier count per pole, size, and placement of PM were the key parameters which influenced the ripple content in the developed torque [20]. The torque ripple was the main reason for the noise level of the machine. In the next section, the acoustic analysis was performed for both generators.
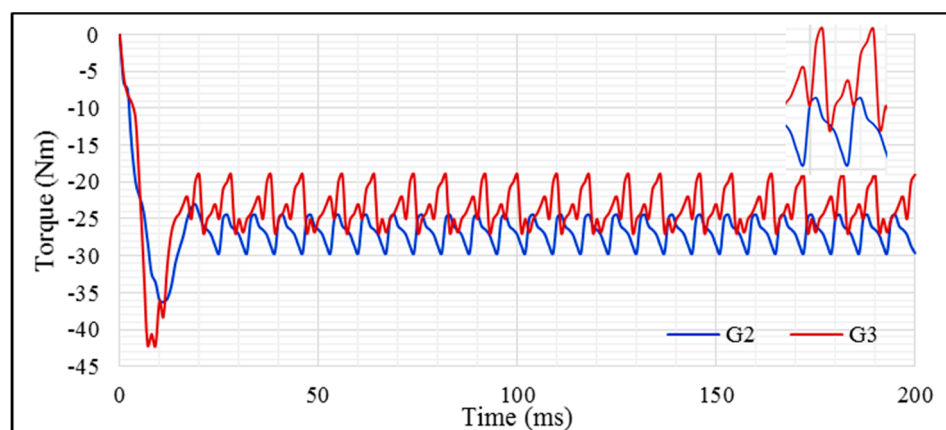
Figure 14. Electromagnetic torque during generating mode for G2 and G3 (operating at rated load).

5.3. Acoustic Analysis

Sound pressure and sound power were the two constraints to compute the local and global acoustic effects [25,26].

In Figure 15, acoustics versus frequency plot measured by decibels are presented for G2 and G3. The maximum noise level was identified from the acoustics versus frequency plot. For (G2) frequency 1036.4 Hz, it was noted that the acoustic pressure of the stator core ranged from -3×10^{-8} MPa to 2.8×10^{-9} MPa (refer to Figure 16a). For (G3) frequency 1066.3 Hz, it was noted that the acoustic pressure of the stator core ranged from -4×10^{-9} MPa to 3×10^{-9} MPa (refer to Figure 16b). The overall machine performances of G2 and G3 are presented in Table 5.
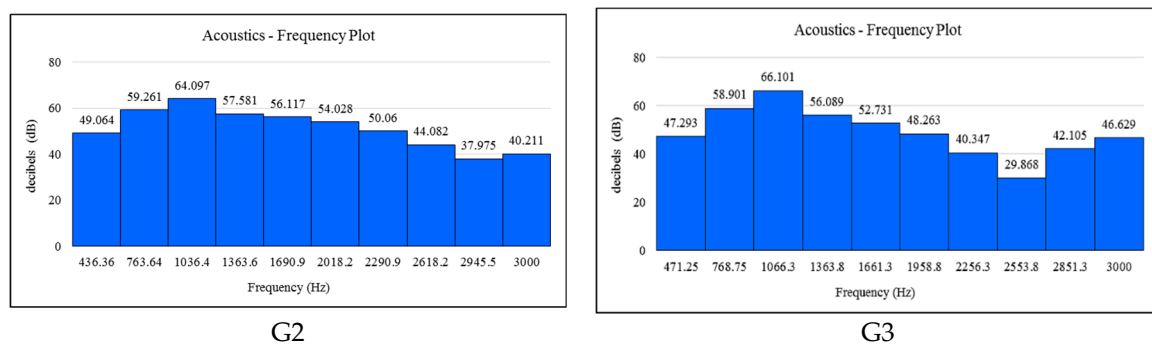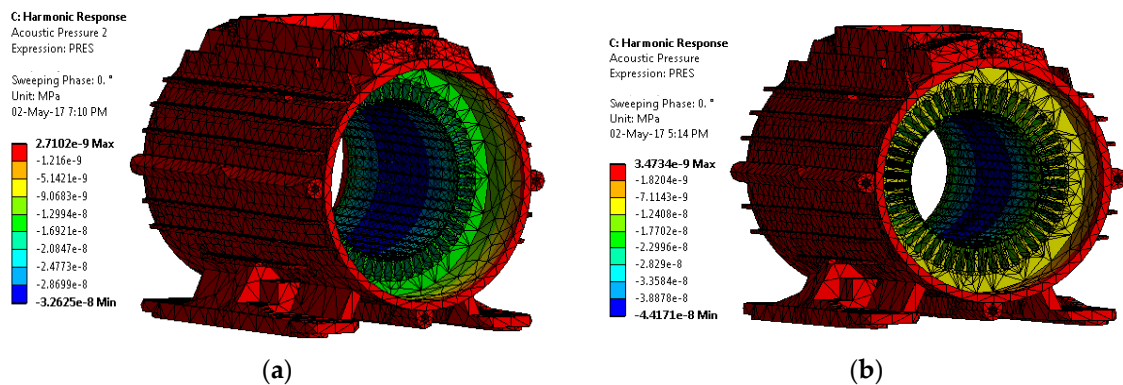

Figure 15. Acoustic versus frequency plot.

Figure 16. Acoustic pressure level for (**a**) G2 and (**b**) G3.

Table 5. Overall performance comparison of G1, G2, and G3 topologies.

Parameter	G1	G2	G3	Remarks
No load induced EMF (V)	281	253.8	263	
Full load voltage (V)	229.1	230.5	228.7	• The voltage regulation of G1 is 3.73 % and 12.52% higher than G3 and G2.
Full load current (A)	21.9	22.2	22.17	
Output power (kW)	5.02	5.12	5.07	• G2 has 8.7% reduced voltage regulation than G3.
Total losses (W)	941	613	995	
%Efficiency	84.2	89.3	83.6	• G2 has a 21.57% higher power/weight ratio than G3.
%Voltage regulation	22.65	10.13	18.9	
kW/kg	0.233	0.496	0.389	• G3 has 5.7% less efficient tan G2.
Maximum winding temperature (°C)	-NE-	100 °C	132 °C	• Noise level of G2 is 3% lesser than G3.
Noise level (dB)	-NE-	64	66	

* NE—not evaluated

6. Cost Estimation

The detailed cost estimation of various components of a 5 kW portable generator for military applications is tabulated in Table 6 (also refer Table A3).

Table 6. Overall cost analysis of PMA-SynRG and IG.

S. No	Material	Grade	Price/kg (approx.)	Part Number	Quantity (kg)		Cost (INR) (max.)	
					G2	G3	G2	G3
1	Non-Oriented AISI Silicon Steel	M-36 29 Ga	80 to 130	-	7	10	910	1300
2	NdFeB	N52	10000 to 12000	-	1.5	nil	18000	-NA-
3	Copper coil	AWG-15	500 to 620	-	nil	3	-NA-	1860
		AWG-16	500 to 620	-	2.5	-NA-	1550	-NA-
4	Copper bar	-	500 to 550	-	nil	2.5	-NA-	1375
5	Capacitor	200 uF/440 V	5600 to 7460	871-B32361B2207J50	nil	2 (count)	-NA-	14920
6	Nomex Insulation	Class F	750 to 1500	-	2	nil	3000	-NA-
		Class H	2500 to 4000	-	nil	2	-NA-	8000
7	Grey cast iron	Grade 350	50 to 80	-Pleae	8	10	640	800
8	Journal bearing	Bearing Steel	100 to 160	6004 6004 ZZ	2 (count)	2 (count)	320	320
9	Fasteners SS 304	IS 1363/DIN 933/BS 1083	25 to 30	M12x20	8 (count)	8 (count)	240	240
10	Fasteners SS 304	IS 1363/DIN 933/BS 1083	55 to 65	M16x30	4 (count)	4 (count)	260	260
11	Fabrication	-	-	-	nil	nil	40000	30000
-	-	-	-	Total (Approx.)	22.5	29	**64920 (926 USD)**	**59075 (842 USD)**

7. Conclusions

This paper investigated the electro-magnetic design analysis of PMA-SynRG with a ferrite rotor (G1), NdFeB rotor (G2), and induction generator (G3). Furthermore, the machines were examined in all aspects, including thermal and acoustic analysis.

From the Analysis

√   Voltage regulation in the G2 rotor was 8.77% less compared to G3.

√   The magnet weight used in G1 was 72.2% higher than G2.

√   The overall weight of G2 was 20.7% and 52% less than G3 and G1, respectively.

√   At rated load, both generators were within the thermal limit for ambient conditions prescribed by the military requirements.

√   The noise level of G2 and G3 was 64 dB and 66 dB, respectively, which is within the range of military standards.

Based on the results, it is clearly evident that both, the PMA-SynRG with NdFeB rotor (G2) and IG are a good choice for military applications (as per military standards), whereas PMA-SynRG with NdFeB (G2) are more suitable within the aspects of power, weight, size, thermal and noise. Likewise, the induction generator is appropriate in the features of power, thermal noise and overall cost. Furthermore, the prototype fabrication process of the machine is under progress.

Appendix A

Table A1. Permanent magnet characteristics [22].

Magnet	Characteristic	Unit	Value
Ferrite	Residual induction Br at 20C	Tesla	0.42
	Energy Product at 20C	kJ/m^3	32.9
	Mass density	kg/m^3	4900
	Max. Working Temperature	°C	300
	Curie Temperature	°C	450
NdFeB	Characteristic	Unit	Value
	Residual induction Br at 20C	Tesla	1.39
	Energy Product at 20C	kJ/m^3	367.4
	Mass density	kg/m^3	7500
	Max. Working Temperature	°C	230
	Curie Temperature	°C	310

Table A2. Thermal properties of the material used.

Material	Density (Kg/m^3)	Specific Heat (J/KgC)	Thermal Conductivity (W/mC)
M36-29 Gauge	7700	490	25
Copper	8954	383.1	386
Nomex 410	1400	1300	0.14
Cast Iron	7272	486	36.3
N52 (NdFeB)	7500	460	7.6

Appendix B

Table A3. References for cost analysis.

S. No	Material	Grade	Price Reference Link	Cost/kg (Rounded Off) Min.	Cost/kg (Rounded Off) Max.
1	Non-Oriented AISI Silicon Steel	M-36 29 Ga	https://www.indiamart.com/proddetail/crgo-electrical-steel-17427063588.html https://www.indiamart.com/proddetail/crgo-transformers-sheet-17382640691.html https://www.indiamart.com/proddetail/crgo-steel-sheet-coil-20408399155.html	**80**	**130**
2	NdFeB	N52	https://www.indiamart.com/proddetail/rare-earth-magnet-rod-5698105812.html https://www.indiamart.com/proddetail/rare-earth-magnets-10573830273.html	10000	12000
3	Copper coil	AWG-15	https://www.indiamart.com/proddetail/copper-winding-coil-15789944088.html https://www.indiamart.com/proddetail/copper-bare-wire-10182933762.html https://www.indiamart.com/proddetail/winding-wire-17856803030.html	500	620
		AWG-16			
4	Copper bar		https://www.indiamart.com/proddetail/phosphorised-copper-bars-12436604612.html https://www.indiamart.com/proddetail/copper-bars-8021904930.html https://www.indiamart.com/proddetail/ec-grade-copper-bars-18801056473.html	500	550
5	Capacitor	200 uF/440 V	https://www.mouser.in/Passive-Components/Capacitors/Film-Capacitors/_/N-5g7r?P= 1z0wqt2Z1ywtais	5600 (1 count)	7460 (1 count)
6	Nomex Insulation	Class F	https://www.indiamart.com/proddetail/nomex-insulation-paper-class-f-19444242012.html https://www.indiamart.com/proddetail/f-class-h-class-insulation-paper-10121409648.html	750	1500
		Class H	https://www.indiamart.com/proddetail/nomex-insulation-paper-class-h-dupont-19444400255.html https://www.indiamart.com/proddetail/h-class-insulation-paper-8938225933.html	2500	4000
7	Grey cast iron	Grade 350	https://www.indiamart.com/proddetail/grey-iron-casting-20401746330.html https://www.indiamart.com/proddetail/grey-iron-casting-20570455262.html	50	80
8	Journal bearing	Bearing Steel	https://www.indiamart.com/proddetail/6004-zz-nsk-ball-bearings-20442772655.html http://www.easysparepart.com/NBC-Ball-Bearing-6004ZZ	100	160
9	Fasteners SS 304 (M12x20)	IS 1363/DIN 933/BS 1083	https://www.pmmetal.com/special-steel-fasteners/stainless-steel-fasteners/stainless-steel-fasteners/ https://www.swiftindustrial.in/downloads/HighTensileFastners.pdf	25 (1 count)	30 (1 count)
10	Fasteners SS 304 (M16x30)			55 (1 count)	65 (1 count)

References

1. Atlascopco. Available online: https://www.atlascopco.com/content/dam/atlas-copco/construction-technique/portableenergy/documents/2_generators/spain/portable-generators/portable-generators-leaflet-english.pdf (accessed on 13 September 2018).
2. Championpowerequipment. 2017. Available online: https://y79961nbs4u2hvbnwronx9zx-wpengine.netdna-ssl.com/wp-content/uploads/2017/09/100490-om-english.pdf (accessed on 9 August 2018).
3. Misron, N.; Rizuan, S.; Vaithilingam, A.; Mailah, N.F.; Tsuyoshi, H.; Hiroaki, Y.; Yoshihito, S. Performance Improvement of a Portable Electric Generator Using an Optimized Bio-Fuel Ratio in a Single Cylinder Two-Stroke Engine. *Energies* **2011**, *4*, 1937–1949. [CrossRef]
4. Matthew, K.S. Electromagnetic Generators for Portable Power Applications. Ph.D. Thesis, University of California, Berkeley, CA, USA, 2005.
5. Home Generators Basics. 2008. Available online: https://www.smps.us/home-generators.html (accessed on 13 September 2018).
6. Norhisam, M.; Syafiq, M.; Aris, I.; Abdul Razak, J. Design and analysis of a single phase slot-less permanent magnet generator. In Proceedings of the International Conference on Power and Energy, Johor Baharu, Malaysia, 1–3 December 2008; pp. 1082–1085.
7. Stegen, K.S. Heavy rare earths, permanent magnets, and renewable energies: An imminent crisis. *Energy Policy* **2015**, *79*, 1–8. [CrossRef]
8. Alkane Resources Ltd. Available online: http://www.alkane.com.au/products/rare-earths-overview/ (accessed on 13 March 2018).
9. Constantinides, S. The Demand for Rare Earth Materials in Permanent Magnets. In Proceedings of the 51st annual Conference on Metullurgists, Niagara Falls, NY, USA, 30 September–3 October 2012; pp. 1–58.
10. Guyonnet, D.; Lefebvre, G.; Menad, N. Guyonnet et al. Rare Earth Elements and High Tech Products. Available online: https://www.cec4europe.eu/wp-content/uploads/2018/09/Chapter_3_3_Guyonnet_et_al_Rare_earth_elements_and_high_tech_products.pdf (accessed on 3 January 2019).
11. Roshanfekr, P.; Lundmark, S.; Thiringer, T.; Alatalo, M. A synchronous reluctance generator for a Wind Application-compared with an interior mounted permanent magnet synchronous generator. In Proceedings of the International Conference on Power Electronics, Machines and Drives (PEMD), Manchester, UK, 8–10 April 2014; pp. 1–5.
12. Hsiao, C.-Y.; Yeh, S.-N.; Hwang, J.-C. Design of high performance permanent-magnet synchronous wind generators. *Energies* **2014**, *7*, 7105–7124. [CrossRef]
13. Vartanian, R.; Deshpande, Y.; Toliyat, H.A. Performance analysis of a rare earth magnet based NEMA frame Permanent Magnet assisted Synchronous Reluctance Machine with different magnet type and quantity. In Proceedings of the International Conference on Electric Machines & Drives (IEMDC), Chicago, IL, USA, 12–15 May 2013; pp. 476–483.
14. Tefera, K.; Tripathy, P.; Adda, R. Electromagnetic and mechanical stress analysis of wind-driven synchronous reluctance generator. *CES Trans. Electr. Mach. Syst.* **2019**, *3*, 107–114. [CrossRef]
15. Alnajjar, M.; Gerling, D. Medium-speed synchronous reluctance generator as efficient, reliable and low-cost solution for power generation in modern wind turbines. In Proceedings of the International Symposium on Power Electronics, Electrical Drives, Automation and Motion, Amalfi, Italy, 20–22 June 2018; pp. 1233–1238.
16. Yamada, A.; Miki, I. Novel Rotor Structure of Permanent Magnet Synchronous Motor with Rare Earth and Ferrite Magnets. In Proceedings of the International Symposium on Power Electronics, Electrical Drives, Automation and Motion, Ischia, Italy, 18–20 June 2014; pp. 1–5.
17. Selmi, M.; Rehaoulia, H. A simple method for the steady state performances of self-excited induction generators. In Proceedings of the International Conference on Electrical Engineering and Software Applications, Hammamet, Tunisia, 21–23 March 2013; pp. 1–4.
18. Chan, T.F. Analysis of a single-phase self-excited induction generator. *Electr. Mach. Power Syst.* **1995**, *23*, 149–162. [CrossRef]
19. Reza, R.M. Synchronous Reluctance Machine (SynRM) Design. Master's Thesis, Royal Institute of Technology Stockholm, Stockholm, Sweden, 2007.
20. Ashkezari, J.D.; Khajeroshanaee, H.; Niasati, M. Optimum design and operation analysis of permanent magnet-assisted synchronous reluctance motor. *Turk. J. Electr. Eng. Comput. Sci.* **2017**, *7*, 7105–7124.

21. Boroujeni, S.T.; Haghparast, M.; Bianchi, N. Optimization of flux barriers of line-start synchronous reluctance motors for transient- and steady-state operation. *Electr. Power Compon. Syst.* **2015**, *43*, 3–17. [CrossRef]

22. Massimo, B.; Nicola, B. Interior PM machines using ferrite to replace rare-earth surface PM machines. *IEE Proc. Electr. Power Appl.* **2014**, *50*, 979–984.

23. Pavan, A.; Sathyanarayanan, N.; Rajeshkumar, R.; Lenin, N.C.; Sivakumar, R. Thermal analysis of a 3 phase, 550 w switched reluctance machine. *Int. J. Appl. Eng. Res.* **2015**, *10*, 86–90.

24. Staton, D.A.; Cavagnino, A. Convection heat transfer and flow calculations suitable for electric machines thermal models. *IEEE Trans. Ind. Electron.* **2008**, *55*, 3509–3516. [CrossRef]

25. Tong, W. *Mechanical Design of Electric Motors*; CRC Press: London, UK, 2014; p. 481.

26. Timar, P.L. *Noise and Vibration of Electrical Machines*; Elsevier Science Ltd.: Amsterdam, The Netherlands, 1989; p. 355.